Angiographic Features of Transgenic Mice With Increased Expression of Human Serine Protease HTRA1 in Retinal Pigment Epithelium

Sandeep Kumar,[1] Zachary Berriochoa,[1] Balamurali K. Ambati,[1,2] and Yingbin Fu[1,2]

[1]Department of Ophthalmology and Visual Sciences, University of Utah Health Sciences Center, Salt Lake City, Utah, United States
[2]Department of Neurobiology and Anatomy, University of Utah Health Sciences Center, Salt Lake City, Utah, United States

Correspondence: Yingbin Fu, Department of Ophthalmology and Visual Sciences, University of Utah Health Sciences Center, 65 Mario Capecchi Drive, Salt Lake City, UT 84132, USA;
yingbin.fu@hsc.utah.edu.

Submitted: August 21, 2013
Accepted: May 9, 2014

Citation: Kumar S, Berriochoa Z, Ambati BK, Fu Y. Angiographic features of transgenic mice with increased expression of human serine protease HTRA1 in retinal pigment epithelium. *Invest Ophthalmol Vis Sci*. 2014;55:3842–3850. DOI: 10.1167/iovs.13-13111

Purpose. Polypoidal choroidal vasculopathy (PCV) is characterized by a branching vascular network (BVN) of choroid that terminates in polypoidal dilations. We have previously reported the generation of the first PCV model by transgenically expressing human HTRA1 (*bHTRA1*$^+$), a multifunctional serine protease, in mouse RPE. The purpose of this study was to perform a comprehensive examination of the PCV phenotypes (e.g., lesion type and distribution) of *bHTRA1*$^+$ mice by a variety of in vivo imaging techniques.

Methods. We generated improved *bHTRA1*$^+$ mice with a more consistent phenotype. Transgenic mice were examined by indocyanine green angiography (ICGA), fluorescein angiography, funduscopy, and spectral-domain optical coherence tomography. In particular, we performed ICGA by tail vein injection of ICG to obtain high-quality ICGA comparable to human studies in terms of the three phases (early, middle, and late) of angiography.

Results. The polyps can be detected in the early "fill-in" phase of ICGA, and most lesions become visible in the middle phase and are more distinct in the late phase with the fading of surrounding vessels. In addition to the two key features of PCV (polypoidal dilations and BVNs), *bHTRA1*$^+$ mice exhibit other features of PCV (i.e., late geographic hyperfluorescence, pigment epithelial detachment, and hyperfluorescent plaque). Polypoidal lesions appear as reddish orange nodules on funduscopy.

Conclusions. Transgenic *bHTRA1*$^+$ mice exhibit a rich spectrum of "clinical" features that closely mimic human PCV. This animal model will serve as an invaluable tool for future mechanistic and translational studies of PCV and other forms of choroidal vasculopathies.

Keywords: polypoidal choroidal vasculopathy, HTRA1, indocyanine green angiography, late geographic hyperfluorescence, pigment epithelial detachment

Polypoidal choroidal vasculopathy (PCV) is characterized by a network of branching vessels with terminal polypoidal dilations in the choroidal vasculature.[1,2] Indocyanine green angiography (ICGA) is used for the diagnosis of PCV when routine ophthalmoscopic examination reveals serosanguineous maculopathy, visible reddish orange subretinal nodules, spontaneous massive subretinal hemorrhage, and hemorrhagic pigment epithelial detachment (PED).[1–5] In addition, other clinical markers such as late geographic hyperfluorescence (LGH)[6–8] and hyperfluorescent plaque[7,9,10] have been visualized in PCV eyes. Polypoidal choroidal vasculopathy is frequently associated with recurrent serosanguineous detachments of RPE and retina, with leakage and bleeding from the polypoidal components.[1,11,12] It is found in 22% to 55% of Asians with neovascular AMD[11,13] and in almost every African American with neovascular AMD.[1] In Caucasians, PCV is present in 4% to 10% of AMD cases[10,13] and in approximately 85% of patients with hemorrhagic or exudative PED.[10] Polypoidal choroidal vasculopathy is considered a variant of occult-type choroidal neovascularization (CNV) (or type 1 neovascularization),[1,3] in which the abnormal vessels are located in the sub-RPE space. The etiology and pathogenesis of PCV are not well understood. Moreover, current anti-VEGF therapy is not as effective in treating PCV as with classic CNV (or type 2 neovascularization).[14–18] A well-characterized animal model of PCV will service as an invaluable tool for future mechanistic and translational studies of this disease.

We recently reported the generation of the first PCV model by transgenically expressing human HTRA1 (*bHTRA1*$^+$), a multifunctional serine protease, in mouse RPE.[19] We demonstrated that increased HTRA1 induced characteristic features of PCV, including branching networks of choroidal vessels and polypoidal lesions. Ultrastructural study revealed degeneration of both the elastic lamina and tunica media of choroidal vessels, as well as the degradation of the elastic lamina of Bruch's membrane in *bHTRA1*$^+$ mice.

In this work, we generated an improved transgenic HTRA1 mouse model Tg44 with more consistent PCV phenotypes. We performed a comprehensive characterization of the PCV phenotypes (e.g., lesion type and distribution) of *bHTRA1*$^+$ mice by ICGA, fluorescein angiography (FA), funduscopy, and spectral-domain optical coherence tomography (SD-OCT). Our study showed that *bHTRA1*$^+$ mice exhibit not only the two key features of PCV (polypoidal dilations and branching vascular networks [BVNs]) but also additional features of PCV (e.g., LGH, PED, and hyperfluorescent plaque).

TABLE. Distribution of Angiographic Features in 124 Tg44 Mice (65 Males and 59 Females) Based on IV-ICGA

Variable	Male	Female	Overall	Male–Female Ratio	*P* Value
Polyps	100.0	100.0	100.0	1.00	...
BVNs	100.0	100.0	100.0	1.00	...
LGHs	43.1	25.4	34.7	1.69	0.039
Plaques	15.4	6.8	11.3	2.27	0.131
PEDs	21.5	8.5	15.3	2.54	0.044
Single polyp	100.0	100.0	100.0	1.00	...
Cluster polyps	56.9	45.8	51.6	1.24	0.214
String polyps	63.1	64.4	63.7	0.98	0.878

Data are expressed as percentages unless otherwise indicated.

METHODS

Reagent

Purified full-length $(His)_6$-tagged human HTRA1 protein was purchased from Pierce Biotechnology (Rockford, IL, USA). Eye tissues from human donors (age range, 50–73 years) without AMD history were obtained from Utah Lions Eye Bank (Salt Lake City, UT, USA).

Animals

Transgenic *hHTRA1*$^+$ Tg44 mice were generated using a similar strategy as in our previous work[19] except that a cytomegalovirus enhancer was not included and a woodchuck posttranscriptional regulatory element (WPRE) was inserted before the bovine growth hormone poly(A) signal. The Tg44 mice were generated in the C57Bl/6 × CBA background and were crossed eight times with CD1 mice (Charles River Laboratories, Hollister, CA, USA), although we started to analyze phenotypes from the fourth generation. Animal experiments were conducted according to protocols approved by the Institutional Animal Care and Use Committee and were performed in accordance with the ARVO Statement for the Use of Animals in Ophthalmic and Vision Research.

Western Blot and Immunohistochemistry

Western blot and immunohistochemistry were performed as described previously.[19] A monoclonal antibody, anti-human HTRA1 (MAB2916, 1:1000; R&D Systems, Minneapolis, MN USA), was used for Western blot experiments. The same anti-human HTRA1 antibody (1:100) and a rabbit anti-bovine RPE65 antibody (1:100)[20] were used for immunohistochemistry. For protein quantification, gel images were captured, and the pixel value of each protein band was obtained in a FluorChem Western Blot Imaging Station with accompanying image analysis software (ProteinSimple, Santa Clara, CA, USA). The pixel value in arbitrary units was plotted against the amount of recombinant HTRA1 protein to construct a standard curve, which was then used to extrapolate the amount of human HTRA1 in human and mouse RPE samples.

Angiography, Funduscopy, and SD-OCT

For all in vivo imaging, mice were anesthetized by intraperitoneal (IP) injection of a combination of ketamine (65–100 mg/kg), xylazine (10–20 mg/kg), and acepromazine (1–3 mg/kg). Pupils were dilated with 1% tropicamide (Bausch & Lomb, Incorporated, Rochester, NY, USA). Funduscopic examinations were performed with Micron III from Phoenix Research Laboratories (San Ramon, CA, USA). Fluorescein angiography, ICGA, and SD-OCT were performed with an Heidelberg Retina Angiograph (HRA)-OCT device (Spectralis) from Heidelberg Engineering (Heidelberg, Germany). Indocyanine green (2 mg/kg; Pfaltz & Bauer, Waterbury, CT, USA) or fluorescein sodium (AK-FLUOR, 10 mg/kg; Akorn, Inc., Lake Forest, IL, USA) were delivered into mice by tail vein injection. Immediately after injection, time-course ICGA or FA was recorded. Indocyanine green and fluorescein sodium were injected either individually or together. For SD-OCT, mice were placed on a custom-made table. The OCT sessions were performed at 30° field of view using the high-resolution mode (signal quality, ≥24 dB) with scan speed of 40,000 A-scans per second. The image scaling x and z were 1.10 μm per pixel and 3.87 μm per pixel, respectively. The optimal focus depth was approximately 47 diopters. Axial resolution was 7 μm optical and 3.5 μm digital. We have found that mouse OCT scans in black on white (reflective layers look black) provide better contrast for retinal, RPE, and choroidal layers than in white on black. Accordingly, we exported all OCT images in black on white. We named the various reflective bands according to published mouse OCT studies[21,22] comparing retinal histology with SD-OCT in various mouse models of retinal degeneration. Angiography, funduscopy, and SD-OCT data were exported as 8-bit grayscale image files and were processed with Photoshop 7 (Adobe Systems, San Jose, CA, USA).

Statistical Analysis

Statistics in the Table were calculated by the χ^2 test and elsewhere by Student's *t*-test. $P < 0.05$ was considered statistically significant.

RESULTS

Expression of Human HTRA1 in Mouse RPE

We generated two mouse lines (*hHTRA1*$^+$ Tg73 and Tg44) overexpressing human HTRA1 in mouse RPE. The phenotype of Tg73 has been extensively characterized and described in our previous publication.[19] Both mouse lines exhibit similar PCV phenotypes. We used the Tg44 line in this study because it has a more consistent phenotype. The Tg44 transgene was driven by the RPE-specific human vitelliform macular dystrophy 2 promoter.[23] The absolute levels of human HTRA1 in transgenic *hHTRA1*$^+$ and normal human (age range, 50–60 years) RPE were measured by Western blot with a monoclonal antibody (anti-human HTRA1) that recognizes human but not mouse HTRA1. By comparison with purified $(His)_6$-tagged recombinant human HTRA1 standards, the mean (SEM) human HTRA1 level was determined to be 1.35 (0.03) ng per 10 μg lysate in *hHTRA1*$^+$ RPE, which is approximately 3.1 times that of human RPE (0.43 [0.02] ng per 10 μg lysate) (Figs. 1A–C). Thus, Tg44 has a slightly lower expression level of human HTRA1 (1.46 times) compared with the previous Tg73 line (1.97 ng per 10 μg lysate).[19] Similar to Tg73, HTRA1 was expressed at the basal side (Fig. 1D, white arrows at the bottom right) of RPE (in red, labeled by an antibody against an RPE marker protein [RPE65][20]), Bruch's membrane (white arrowheads), and choroid (yellow arrows) of *hHTRA1*$^+$ mice, suggesting that transgenic HTRA1 was secreted from the basal RPE toward the Bruch's membrane and choroid.

Characterization of PCV Lesion Types by Time-Course Intravenous ICGA

Transgenic mice were bred into either C57BL/6 or CD1 backgrounds. The albino CD1 background was selected to

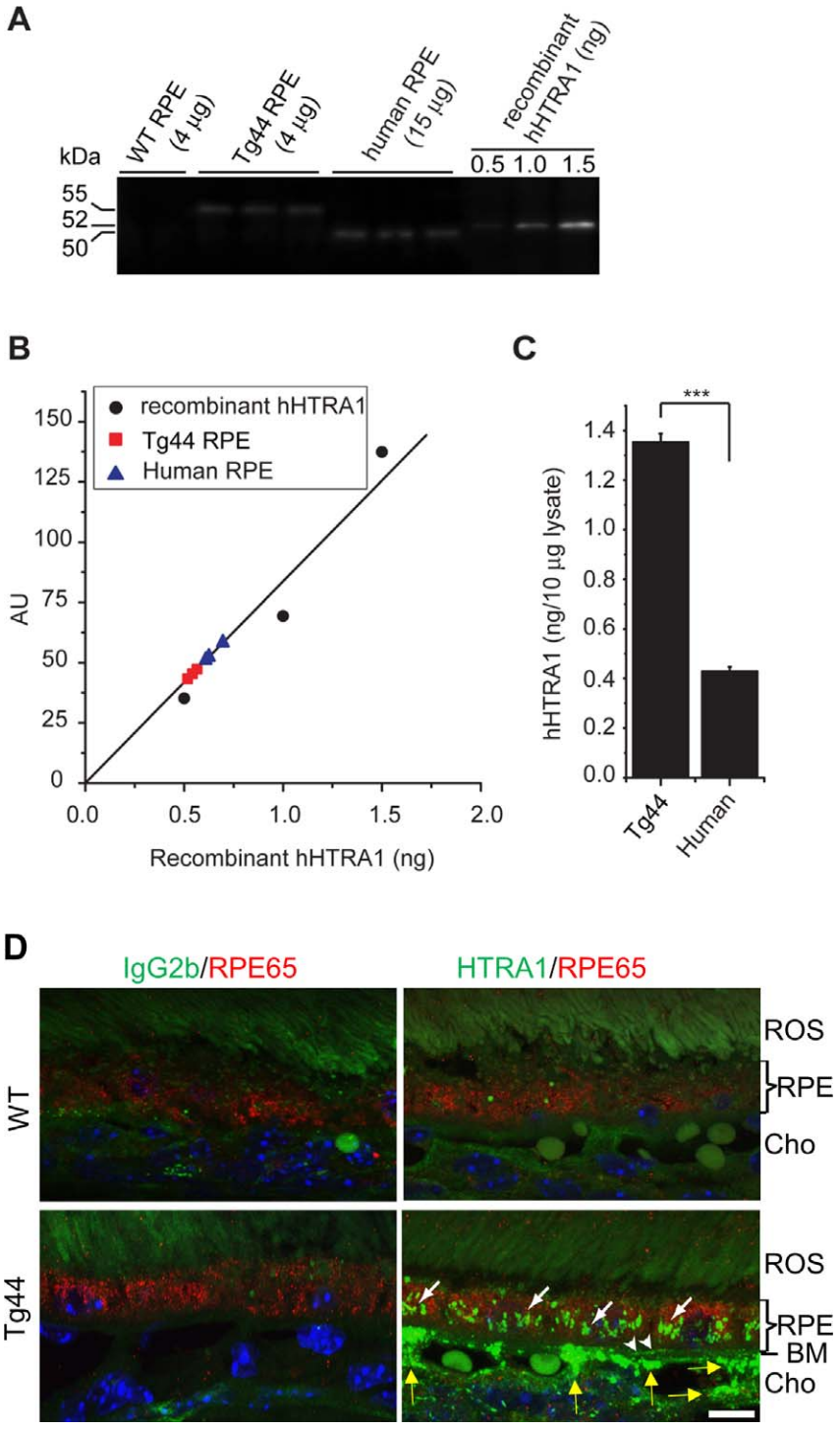

Figure 1. Expression of human HTRA1 in mouse RPE. (**A**) Western blot analysis of human HTRA1 expression in RPE and choroid of Tg44 mice. The Western blot shows the relative levels of human HTRA1 signal from 4 μg RPE and choroid lysate of Tg44 mice ($n = 3$) and 15 μg lysate of human RPE ($n = 3$). $(His)_6$-tagged recombinant human HTRA1 protein (approximately 52 kDa) was used as the standard (in nanograms). The myc-$(His)_6$-tagged transgenic HTRA1, $(His)_6$-tagged recombinant HTRA1, and native HTRA1 (from human RPE and choroid) ran at 55, 52, and 50 kDa, respectively. (**B**) The pixel values of the recombinant protein bands in (**A**) in arbitrary units (AU) were plotted against the protein amounts to construct a standard curve. The expression levels of human HTRA1 in Tg44 mice and human RPE were determined according to their AU and the standard curve. (**C**) Comparison of human HTRA1 protein levels in Tg44 mice and human RPE ($n = 3$). Data are expressed as means (SEMs). $^{***}P < 0.001$. (**D**) Retinal sections from WT and Tg44 mice immunostained with a mouse anti-human HTRA1 antibody (*green*) or the isotype control mouse IgG2b together with a rabbit anti-bovine RPE65 antibody (*red*).[20] Nuclei were stained with 4′,6-diamidino-2-phenylindole (DAPI; *blue*). Transgenic HTRA1 was detected at the basal side of RPE (*white arrows*), Bruch's membrane (*white arrowheads*), and choroid (*yellow arrows*) of *hHTRA1*$^+$ mice. BM, Bruch's membrane; Cho, choroid; ROS, rod outer segment. *Scale bar*: 10 μm.

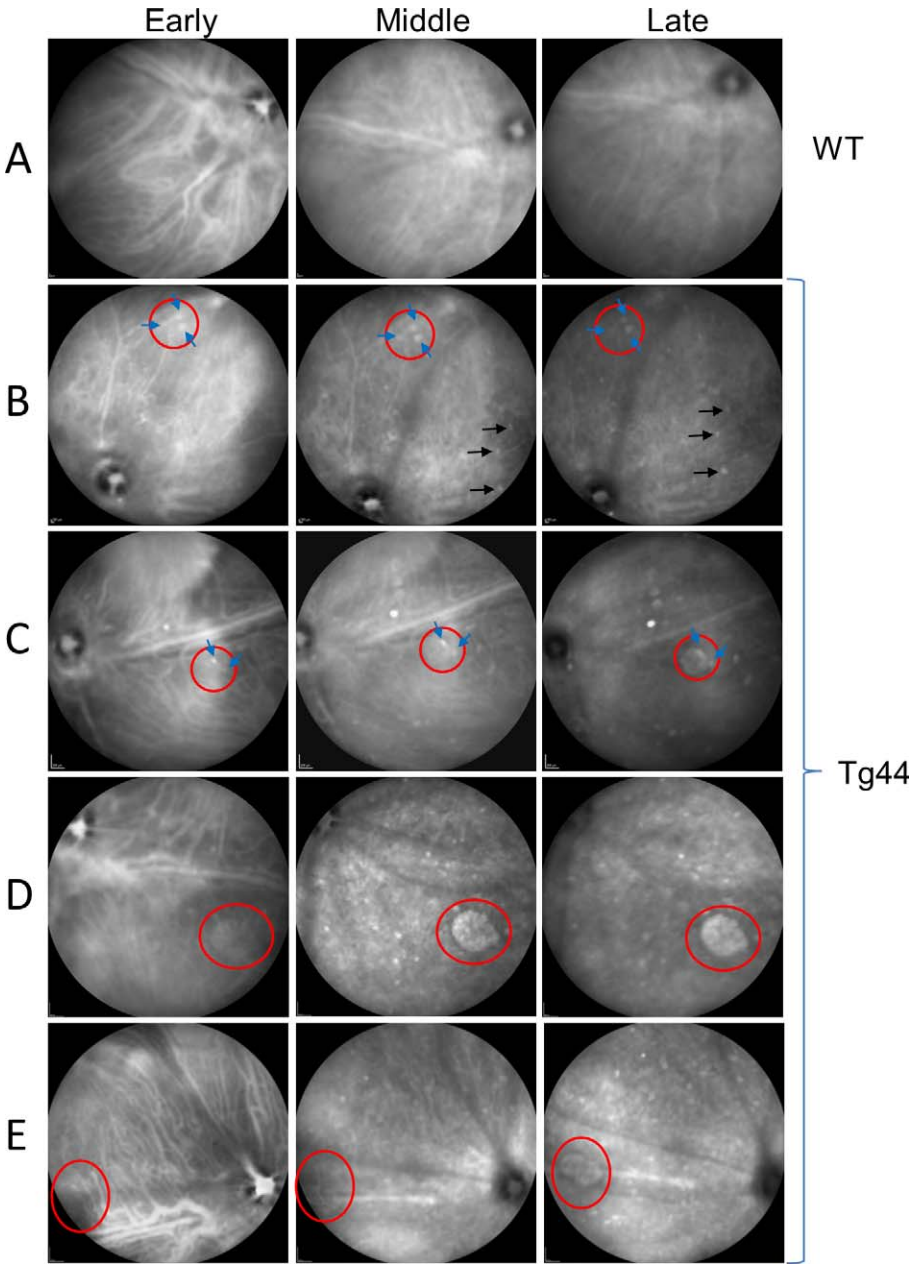

FIGURE 2. Angiographic features of Tg44 mice on time-course IV-ICGA. The early, middle, and late phases of ICGA were recorded for WT control (**A**) and Tg44 mice (**B–E**). The Tg44 mice developed a variety of phenotypes related to PCV, polyp dilations ([**B**, **C**], *blue arrows*), BVNs ([**B–D**], *red circles on the left*), LGHs ([**C**, **D**], *red circles*), and hyperfluorescent plaques ([**E**], *red circle*).

facilitate ICGA imaging.[24,25] The phenotypes were broadly similar in the two genetic backgrounds. We examined 131 Tg44 mice (71 males and 60 females; age range, 1–14 months) and 55 wild-type (WT) littermate controls (30 males and 25 females) using ICGA, FA, SD-OCT, and funduscopy.

Indocyanine green angiography is the recommended method for diagnosing PCV in the clinic due to its capability to image the posterior choroidal vasculature.[4] Previously, we performed ICGA on the Tg73 mice by delivering ICG via IP injection (IP-ICGA).[19] However, we found that the time course was highly variable from mouse to mouse, likely due to the variable absorption of the ICG dye from the body cavity in the abdomen.[25] This makes it difficult to obtain the early, middle, and late phases of ICGA that are comparable with human studies performed by intravenous (IV) injection (i.e., IV-ICGA). Because the angiographic features of the three phases of IV-ICGA are very useful for characterizing different types of choroidal lesions in animal models, we switched to IV-ICGA via tail vein injection in this study.

Out of 131 Tg44 mice, 124 (94.7%) showed characteristic features of PCV, including a BVN and terminal polypoidal dilations (polyps), with the age at onset varying between 4 and 5 weeks. By using IV-ICGA, we studied the PCV lesion types and their distribution in these 124 PCV^{+} mice (Table; Fig. 2). Branching vascular networks (Figs. 2B–D, red circles on the left) and polyps (Figs. 2B, 2C, blue arrows) begin to appear approximately 1 minute after ICG injection in the early phase (0–4 minutes) and become more distinct in the middle phase (6–15 minutes) and late phase (18–22 minutes) with the fading of the choroidal vasculature. More lesions started to appear in

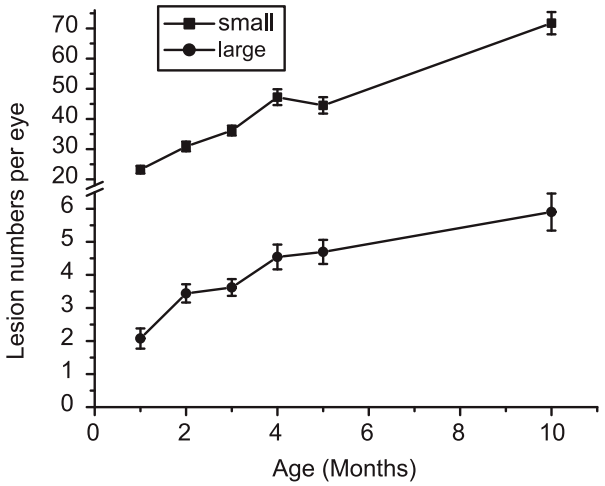

FIGURE 3. The PCV lesion numbers increased during a 10-month period in Tg44 mice. The numbers of small (≤100 μm) and large (>100 μm) lesions per eye were counted at age 1 ($n = 40$), 2 ($n = 50$), 3 ($n = 76$), 4 ($n = 46$), 5 ($n = 36$), and 10 ($n = 41$) months. Data are expressed as means (SEMs).

the middle phase (black arrows). In the late phase (18–22 minutes), polyps began to fade with the disappearance of choroidal vessels. A previous clinical study[26] in human patients has classified PCV lesions into the three groups of single, cluster (more than two polyps in a group), and string (three or more polyps in a line). We found that the single polyp is the most common type of PCV lesion in PCV$^+$ Tg44 mice (100.0%), followed by the string (63.7%) and cluster (51.6%) polyps. The cluster polyps were associated with increased frequency of hemorrhage and high risk of severe visual loss in human PCV patients.[27]

In addition to BVNs and polyps, 34.7% of PCV$^+$ Tg44 mice also exhibited LGH (Table; Figs. 2C, 2D, red circles), which is frequently associated with PCV in human patients.[6,7] These hyperfluorescent lesions start to appear in the middle phase and exhibit a clearly demarcated geographic margin in the late phase of ICGA. Figure 2D shows an example of delayed filling of ICG with pooling of the dye, which becomes strongly hyperfluorescent in the middle phase and retains its hyperfluorescence in the late phase. The LGHs are associated with a BVN, which shows up in the early phase (Fig. 2D, red circle on the left). Polyps were also frequently observed in LGHs (two polyps in Fig. 2C, indicated by blue arrows, and multiple polyps in Fig. 2D). A low percentage of Tg44 mice (11.3%) demonstrates hyperfluorescent plaque on ICGA (Fig. 2E, red circle). In comparison to LGH, the plaques have fuzzier and blunt margins, as well as weak fluorescence, on ICGA.[7] The lower incidence of plaques in Tg44 mice is consistent with the lower incidence of plaques in human PCV but the higher incidence in exudative AMD.[7]

Pigment epithelial detachment was detected in the lesion area in 15.3% of PCV$^+$ mice. The PEDs can be seen on SD-OCT (see Fig. 5C below, red bracket in the middle and magnified at the bottom). The PCV lesion size varies from approximately 50 μm to approximately 700 μm. The largest linear dimensions of LGH, plaque, and PED are 690, 610, and 850 μm, respectively. None of the above features (polyps, BVNs, LGHs, PEDs, and plaques) were observed in WT littermates. The incidence of PCV is higher in males than females among Asians (71% male), while the opposite is true for Europeans (75% female).[1] We observed no such sex difference in Tg44 mice with PCV phenotypes (65 males and 59 females). However, male Tg44 mice have more severe phenotypes such as LGH (1.7 ratio of males to females, $P = 0.039$) and PED (2.5 ratio of males to females, $P = 0.044$) than females (Table). Although males also have a higher incidence of plaques (2.3 ratio of males to females) and cluster polyps (1.2 ratio of males to females), the differences were not significant. We have measured the progression of lesion numbers during a 10-month period (age range, 1–10 months) (Fig. 3). Lesion numbers per eye increased over time for both small lesions (≤100 μm) and large lesions (>100 μm). It is interesting that the numbers of both small lesions and large lesions increased approximately three times during 10 months ($P < 0.001$).

Characterization of Tg44 Mice by Funduscopy, SD-OCT, and FA

The polypoidal lesions in human PCV often appear as reddish orange nodules on color fundus images. Indeed, we observed such nodules in Tg44 mice corresponding to lesion positions (Fig. 4B, white arrowheads). A cluster of polypoidal lesions, which faded at the late phase of ICGA, appears on the fundus as a cluster of reddish orange nodules (Fig. 4C, red box). Hemorrhagic (Fig. 4B, white stars) and serous (Fig. 4C, white asterisks) PEDs, RPE degeneration (Fig. 4C, yellow arrow), and yellowish hard exudates were observed near the lesion site (Fig. 4B, green arrow).

We used SD-OCT to examine the tomographic features of cluster-type polypoidal dilations and a PED (Fig. 5). The middle polyp of a cluster causes an elevation and detachment in RPE (Fig. 5B, red arrow and bracket). Retinal pigment epithelium degenerates between the middle and right polyps (blue bracket). In Figure 5C, a PED (red bracket in the middle and magnified at the bottom) was detected in a PCV lesion on ICGA (red arrow). In contrast, RPE, choroidal, and retinal layers were normal in the WT control (Fig. 5A).

The ICGA lesions are often not visible on FA, suggesting that they are located in choroid or RPE. Figure 6 shows a case study for a 4-month-old Tg44 mouse using ICGA, FA, funduscopy, and SD-OCT. Numerous small lesions and one large LGH lesion are visible on ICGA but not on FA. The large LGH lesion is also visible on funduscopy as reddish orange nodules (red box). Spectral-domain optical coherence tomography localized the lesion in choroid, which is indicated by the dense choroidal hyperreflective structure between the yellow arrow and the right blue arrow (Fig. 6, two blue arrows indicate the margin of the lesion, and the yellow arrow indicates the notch of the lesion). One polyp located on the right border of the LGH (purple arrow) invades into the sub-RPE space (red bracket on OCT, purple arrow), which is similar to OCT findings in human PCV.[28]

DISCUSSION

We have examined a total of 131 Tg44 mice (71 males and 60 females). We found that the two key features of PCV (polypoidal dilations and BVNs) were present in 124 Tg44 mice by IV-ICGA. On funduscopy, polypoidal lesions appeared as reddish orange nodules. Spectral-domain optical coherence tomography localized the lesions in choroid, while round protrusions of RPE could be detected, which is consistent with polypoidal lesions. These phenotypes share remarkable similarities to the well-established clinical features of human PCV.[1] The Tg44 mice also exhibited additional features that are present in PCV and wet-type AMD (e.g., LGH, plaque, and PED). Currently, no other animal models exist with all these phenotypes. This rich spectrum of phenotypes makes the *bHTRA1*$^+$ mice an ideal animal model for a wide range of studies (e.g., drug screening). It is intriguing that male Tg44

Investigative Ophthalmology & Visual Science

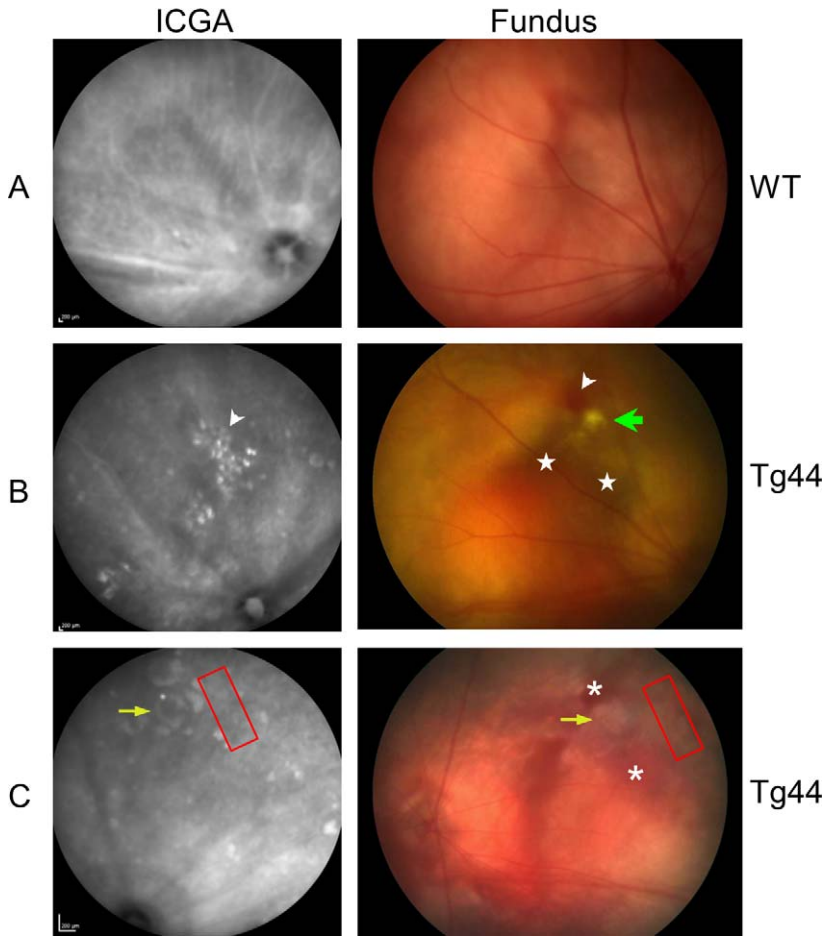

Figure 4. Funduscopic features of PCV lesions. Funduscopic examination was performed in WT control and Tg44 mice. In Tg44 mice, reddish orange nodules, which correspond to PCV lesion structures, are indicated ([**B**], *white arrowhead*; [**C**], *red box*). Hemorrhagic ([**B**], *white stars*) and serous ([**C**], *white asterisks*) PEDs, RPE degeneration ([**C**], *yellow arrow*), and yellowish hard exudates were observed near the lesion site ([**B**], *green arrow*).

mice exhibit more severe types of lesions (e.g., LGH and PED) than females. This is reminiscent of the higher incidence of PCV in males than females among Asians, although the opposite is true for Europeans.[1] One possible explanation is that estrogen has a role in the maintenance of normal extracellular matrix turnover in the eye.[29]

As shown in our previous work,[19] the most parsimonious explanation for the development of PCV in our model is that it is initiated by HTRA1-mediated degradation of extracellular matrix proteins in the RPE–choroid region. HTRA1 is known to degrade many extracellular matrix proteins (e.g., fibronectin and fibromodulin).[30–33] In addition, we showed that purified recombinant human HTRA1 could degrade elastin.[19] As an essential component of Bruch's membrane and the choroid vessel wall, elastin degradation may directly contribute to PCV pathology. Future work in performing histopathological studies on the different types of lesions in Tg44 mice should help clarify the pathophysiological mechanism on how increased HTRA1 leads to PCV. Moreover, these studies will help us understand the pathogenesis of different types of lesions (e.g., polyps, BVNs, and LGHs), which are understudied in human cases.

Indocyanine green angiography is considered the gold standard for the diagnosis of PCV. Although time-course ICGA by IV injection is widely used in the clinic, ICGA by IP injection is commonly used in animal research. Although it is much easier to introduce ICG to the mouse vasculature by IP, we found that it is difficult to obtain reproducible ICGA time-course images by IP-ICGA.[25] In contrast, ICGA via tail vein injection provides high-quality ICGA time-course images comparable to human studies in terms of the early, middle, and late phases (Fig. 2). By using this technique, the polyps can be detected in the early "fill-in" phase of ICGA, and most lesions become visible in the middle phase and are more distinct in the late phase with the fading of surrounding vessels. This technique is also useful to distinguish between different types of lesions (e.g., LGHs versus plaques) (Figs. 2C, 2D versus Fig. 2E). By comparison, we used IP-ICGA for our previous study,[19] which yields far less information on the different types of lesions. The characterization and "diagnosis" are also more accurate with IV-ICGA. To the best of our knowledge, this is the first study to use IV-ICGA in mouse models. Based on our experience, we suggest that time-course IV-ICGA should become standard practice in the examination of phenotypes related to AMD in animal models.

The principal therapies for PCV are laser photocoagulation, photodynamic therapy (PDT), and anti-VEGF drugs (ranibizumab or bevacizumab).[1,34] Anti-VEGF treatment for PCV led to improved visual acuity; however, it is not as effective as it is in wet AMD.[18,35,36] Ranibizumab or bevacizumab may reduce the fluid from PCV, but they show limited effect for diminishing polyps and associated BVNs.[14,15,18,35] The therapeutic effect decreased over time in patients with choroidal vascular hyperpermeability.[35,37] The best reported treatment combines PDT with anti-VEGF drugs.[1,34] However, PDT can cause

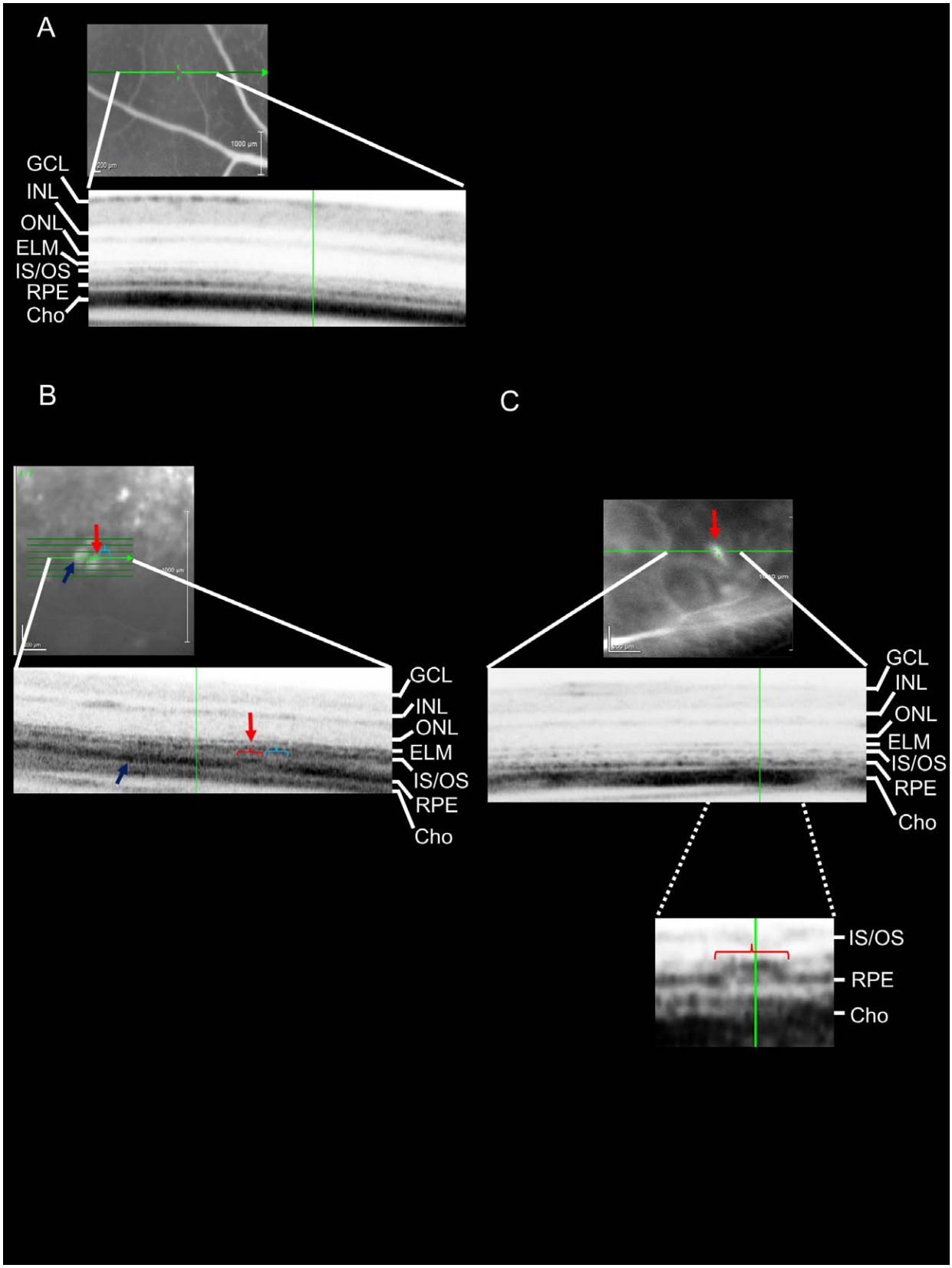

Figure 5. Tomographic features of PCV lesions. Spectral-domain optical coherence tomography was used to examine WT controls (**A**), cluster polyps (**B**), and PEDs (**C**) in Tg44 mice. (**B**) The *blue arrow* indicates the start of the lesion. The *red bracket* indicates an RPE bump, which corresponds to the *middle* polyp (*red arrow*). The *blue bracket* indicates RPE degeneration between the *middle* and *right* polyps. (**C**) The *red bracket* indicates a PED located in a PCV lesion area (*red arrow*). Shown at the *bottom* is a magnified (×3) region of the PED. Detachment of RPE can be clearly seen. Cho, choroid; ELM, external limiting membrane; GCL, ganglion cell layer; INL, inner nuclear layer; IS/OS, the transition zone between the inner and outer segments (also referred to in human clinical literature as the inner segment ellipsoid[40]); ONL, outer nuclear layer.

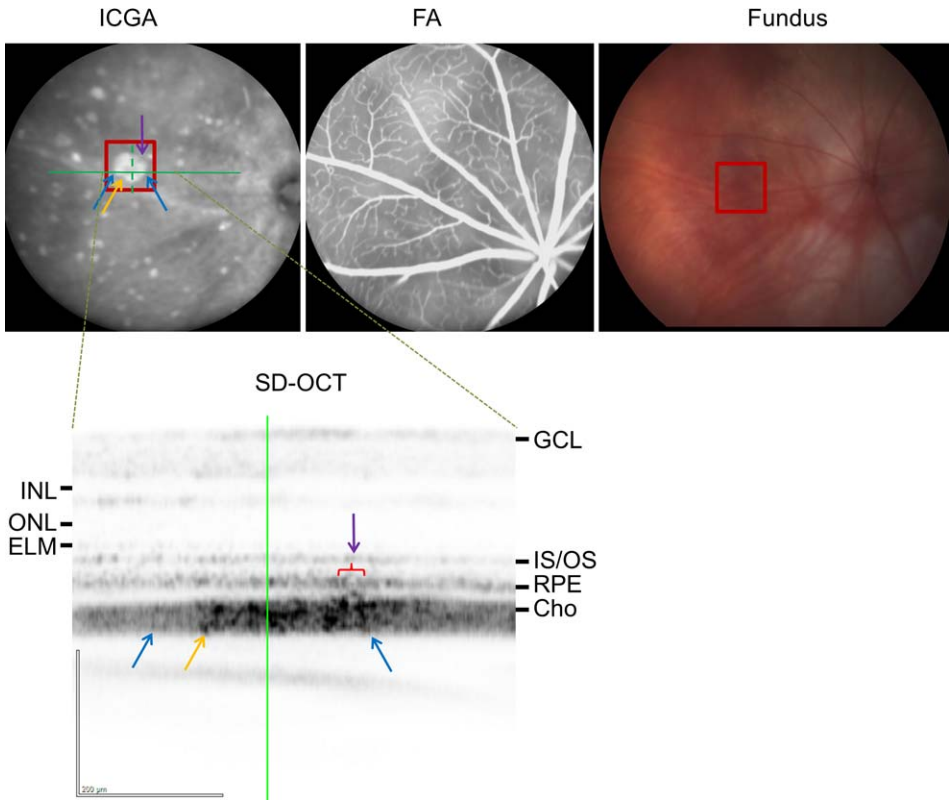

FIGURE 6. A representative 4-month-old Tg44 mouse was examined by ICGA, FA, funduscopy, and SD-OCT. The *red box* indicates an LGH-type lesion on ICGA and funduscopy. The OCT scan line is indicated by a *green horizontal line* on the ICGA image. Two *blue arrows* mark the boundary of the LGH lesion. A *yellow arrow* points to a notch of the LGH, which corresponds to the beginning of a choroidal hyperreflective structure on OCT. A *red bracket* on OCT indicates the location of a polyp (*purple arrow* on ICGA) inside the sub-RPE space. Note that the junction of the IS/OS (the transition zone between the inner and outer segments) and the RPE layers are present, suggesting no significant RPE atrophy.

subretinal hemorrhage, resulting in a poor visual prognosis. Another major concern regarding PDT is the high rate of recurrence or the development of new polypoidal lesions.[1] Moreover, RPE-derived VEGF is essential in maintaining the choriocapillaris, suggesting that long-term blockade of VEGF signaling in retinal diseases may have detrimental adverse effects.[38,39] Therefore, the development of novel drugs that prevent or reduce polypoidal lesions could have a considerable impact on the current therapeutic strategy. A well-characterized animal model of PCV will serve as an invaluable tool for future research.

Acknowledgments

The authors thank Jian-Xing. Ma for the RPE65 antibody and thank Paul Bernstein and the Yingbin Fu laboratory members for discussions and comments on the manuscript.

Supported by National Institutes of Health Grants 1R01EY022901 and 5P30EY014800, a Career Development Award from Research to Prevent Blindness, the Carl Marshall Reeves & Mildred Almen Reeves Foundation, and an unrestricted grant to the Department of Ophthalmology and Visual Sciences, University of Utah Health Sciences Center, from Research to Prevent Blindness.

Disclosure: **S. Kumar**, None; **Z. Berriochoa**, None; **B.K. Ambati**, None; **Y. Fu**, P

References

1. Imamura Y, Engelbert M, Iida T, Freund KB, Yannuzzi LA. Polypoidal choroidal vasculopathy: a review. *Surv Ophthalmol*. 2010;55:501–515.
2. Spaide RF, Yannuzzi LA, Slakter JS, Sorenson J, Orlach DA. Indocyanine green videoangiography of idiopathic polypoidal choroidal vasculopathy. *Retina*. 1995;15:100–110.
3. Ciardella AP, Donsoff IM, Yannuzzi LA. Polypoidal choroidal vasculopathy. *Ophthalmol Clin North Am*. 2002;15:537–554.
4. Yannuzzi LA. Indocyanine green angiography: a perspective on use in the clinical setting. *Am J Ophthalmol*. 2011;151:745–751.e1.
5. Koh AH, Chen LJ, Chen SJ, et al; Expert PCV Panel. Polypoidal choroidal vasculopathy: evidence-based guidelines for clinical diagnosis and treatment. *Retina*. 2013;33:686–716.
6. Kim YT, Kang SW, Chung SE, Kong MG, Kim JH. Development of polypoidal choroidal vasculopathy in unaffected fellow eyes. *Br J Ophthalmol*. 2012;96:1217–1221.
7. Kang SW, Chung SE, Shin WJ, Lee JH. Polypoidal choroidal vasculopathy and late geographic hyperfluorescence on indocyanine green angiography. *Br J Ophthalmol*. 2009;93:759–764.
8. Gomi F, Sawa M, Mitarai K, Tsujikawa M, Tano Y. Angiographic lesion of polypoidal choroidal vasculopathy on indocyanine green and fluorescein angiography. *Graefes Arch Clin Exp Ophthalmol*. 2007;245:1421–1427.
9. Coscas G. *OCT in AMD: Optical Coherence Tomography in Age-Related Macular Degeneration*. Heidelberg: Springer; 2009.
10. Lafaut BA, Leys AM, Snyers B, Rasquin F, De Laey JJ. Polypoidal choroidal vasculopathy in Caucasians. *Graefes Arch Clin Exp Ophthalmol*. 2000;238:752–759.
11. Coppens G, Spielberg L, Leys A. Polypoidal choroidal vasculopathy, diagnosis and management. *Bull Soc Belge Ophtalmol*. 2011;317:39–44.

12. Tsujikawa A, Sasahara M, Otani A, et al. Pigment epithelial detachment in polypoidal choroidal vasculopathy. *Am J Ophthalmol*. 2007;143:102–111.
13. Laude A, Cackett PD, Vithana EN, et al. Polypoidal choroidal vasculopathy and neovascular age-related macular degeneration: same or different disease? *Prog Retin Eye Res*. 2010;29:19–29.
14. Gomi F, Sawa M, Sakaguchi H, et al. Efficacy of intravitreal bevacizumab for polypoidal choroidal vasculopathy. *Br J Ophthalmol*. 2008;92:70–73.
15. Lai TY, Chan WM, Liu DT, Luk FO, Lam DS. Intravitreal bevacizumab (Avastin) with or without photodynamic therapy for the treatment of polypoidal choroidal vasculopathy. *Br J Ophthalmol*. 2008;92:661–666.
16. Cho M, Barbazetto IA, Freund KB. Refractory neovascular age-related macular degeneration secondary to polypoidal choroidal vasculopathy. *Am J Ophthalmol*. 2009;148:70–78.e1.
17. Stangos AN, Gandhi JS, Nair-Sahni J, Heimann H, Pournaras CJ, Harding SP. Polypoidal choroidal vasculopathy masquerading as neovascular age-related macular degeneration refractory to ranibizumab. *Am J Ophthalmol*. 2010;150:666–673.
18. Kokame GT, Yeung L, Lai JC. Continuous anti-VEGF treatment with ranibizumab for polypoidal choroidal vasculopathy: 6-month results. *Br J Ophthalmol*. 2010;94:297–301.
19. Jones A, Kumar S, Zhang N, et al. Increased expression of multifunctional serine protease, HTRA1, in retinal pigment epithelium induces polypoidal choroidal vasculopathy in mice. *Proc Natl Acad Sci U S A*. 2011;108:14578–14583.
20. Znoiko SL, Crouch RK, Moiseyev G, Ma JX. Identification of the RPE65 protein in mammalian cone photoreceptors. *Invest Ophthalmol Vis Sci*. 2002;43:1604–1609.
21. Huber G, Beck SC, Grimm C, et al. Spectral domain optical coherence tomography in mouse models of retinal degeneration. *Invest Ophthalmol Vis Sci*. 2009;50:5888–5895.
22. Alex AF, Heiduschka P, Eter N. Retinal fundus imaging in mouse models of retinal diseases. *Methods Mol Biol*. 2013;935:41–67.
23. Esumi N, Oshima Y, Li Y, Campochiaro PA, Zack DJ. Analysis of the VMD2 promoter and implication of E-box binding factors in its regulation. *J Biol Chem*. 2004;279:19064–19073.
24. Janssen A, Hoellenriegel J, Fogarasi M, et al. Abnormal vessel formation in the choroid of mice lacking tissue inhibitor of metalloprotease-3. *Invest Ophthalmol Vis Sci*. 2008;49:2812–2822.
25. Kumar S, Berriochoa Z, Jones AD, Fu Y. Detecting abnormalities in choroidal vasculature in a mouse model of age-related macular degeneration by time-course indocyanine green angiography. *J Vis Exp*. 2014;84:e51061.
26. Cackett P, Wong D, Yeo I. A classification system for polypoidal choroidal vasculopathy. *Retina*. 2009;29:187–191.
27. Uyama M, Wada M, Nagai Y, et al. Polypoidal choroidal vasculopathy: natural history. *Am J Ophthalmol*. 2002;133:639–648.
28. Khan S, Engelbert M, Imamura Y, Freund KB. Polypoidal choroidal vasculopathy: simultaneous indocyanine green angiography and eye-tracked spectral domain optical coherence tomography findings. *Retina*. 2012;32:1057–1068.
29. Elliot SJ, Catanuto P, Espinosa-Heidmann DG, et al. Estrogen receptor beta protects against in vivo injury in RPE cells. *Exp Eye Res*. 2010;90:10–16.
30. Grau S, Richards PJ, Kerr B, et al. The role of human HtrA1 in arthritic disease. *J Biol Chem*. 2006;281:6124–6129.
31. Vierkotten S, Muether PS, Fauser S. Overexpression of HTRA1 leads to ultrastructural changes in the elastic layer of Bruch's membrane via cleavage of extracellular matrix components. *PLoS One*. 2011;6:e22959.
32. Tiaden AN, Klawitter M, Lux V, et al. Detrimental role for human high temperature requirement serine protease A1 (HTRA1) in the pathogenesis of intervertebral disc (IVD) degeneration. *J Biol Chem*. 2012;287:21335–21345.
33. An E, Sen S, Park SK, Gordish-Dressman H, Hathout Y. Identification of novel substrates for the serine protease HTRA1 in the human RPE secretome. *Invest Ophthalmol Vis Sci*. 2010;51:3379–3386.
34. Kang HM, Koh HJ, Lee CS, Lee SC. Combined photodynamic therapy with intravitreal bevacizumab injections for polypoidal choroidal vasculopathy: long-term visual outcome. *Am J Ophthalmol*. 2014;157:598–606.e1.
35. Kang HM, Koh HJ. Long-term visual outcome and prognostic factors after intravitreal ranibizumab injections for polypoidal choroidal vasculopathy. *Am J Ophthalmol*. 2013;156:652–660.
36. Marcus DM, Singh H, Lott MN, Singh J, Marcus MD. Intravitreal ranibizumab for polypoidal choroidal vasculopathy in non-Asian patients. *Retina*. 2013;33:35–47.
37. Sonoda S, Sakamoto T, Otsuka H, et al. Responsiveness of eyes with polypoidal choroidal vasculopathy with choroidal hyperpermeability to intravitreal ranibizumab. *BMC Ophthalmol*. 2013;13:43.
38. Kurihara T, Westenskow PD, Bravo S, Aguilar E, Friedlander M. Targeted deletion of Vegfa in adult mice induces vision loss. *J Clin Invest*. 2012;122:4213–4217.
39. Saint-Geniez M, Kurihara T, Sekiyama E, Maldonado AE, D'Amore PA. An essential role for RPE-derived soluble VEGF in the maintenance of the choriocapillaris. *Proc Natl Acad Sci U S A*. 2009;106:18751–18756.
40. Spaide RF, Curcio CA. Anatomical correlates to the bands seen in the outer retina by optical coherence tomography: literature review and model. *Retina*. 2011;31:1609–1619.

Investigative Ophthalmology & Visual Science